Heliyon 8 (2022) e11317

Contents lists available at ScienceDirect

Heliyon

journal homepage: www.cell.com/heliyon

Research article

A study of the heat-mediated phase transformations of praziquantel hydrates. Evaluation of their impact on the dissolution rate

Duvernis Salazar-Rojas, Teodoro S. Kaufman **, Rubén M. Maggio *

Área de Análisis de Medicamentos, Facultad de Ciencias Bioquímicas y Farmacéuticas, Universidad Nacional de Rosario and Instituto de Química Rosario (IQUIR, CONICET-UNR), Suipacha 531, Rosario S2002LRK, Argentina

ARTICLE INFO

Keywords:
Chemometrics
Hot-stage-MIR
Hydrates
Polymorphism
Praziquantel

ABSTRACT

Comprehensive knowledge of the critical properties of the active pharmaceutical ingredients is a requirement within the modern concept of quality. Praziquantel hemihydrate (HH) and monohydrate (MH) are new solid forms of this antihelmintic agent, which have better solubility properties than the commercial anhydrous solid form (polymorph A). The thermal stability of the hydrates was evaluated, aiming to understand any possible transformation (amorphization, change to a less soluble form).

Therefore, HH and MH were prepared along with the related anhydrous solid forms A and B, and characterized employing solid-state nuclear magnetic resonance, powder X-ray diffraction, mid and near infrared spectroscopy, thermal methods and the intrinsic dissolution rate.

The transformations of HH and MH under thermal stress conditions were monitored through a variable temperature infrared spectroscopy approach, assisted by multivariate curve resolution with alternating least squares (MCR-ALS), finding that HH undergoes a two-step transformation (HH→B→A) to form A, whereas MH dehydrates directly into form A. This was further confirmed by conventional calorimetric methods (differential scanning calorimetry and thermogravimetry) and powder X-ray diffractometry.

The impact of changes in the stressed solid forms and their dissolution rates was also assessed. Significant differences in dissolution performance were found regarding the solid forms produced as a consequence of thermally-induced dehydration.

1. Introduction

Structural or crystal polymorphism is a known property of the solid-state; IUPAC refers to a polymorph as a solid crystalline phase with the same chemical composition of another phase with a different crystal structure [1]. This phenomenon may result in differential physical properties, and even chemical stability [2], among the solid-state forms as a consequence of differences in their behaviour in a given environment [3]. Currently, the definition of polymorphism includes pseudopolymorphism and amorphous phases [4, 5].

Praziquantel (PZQ, Figure 1) is an anthelmintic drug, widely used against schistosomiasis [6]. Its low cost and high tolerance are some of the determinant features behind PZQ being the first choice to treat a wide variety of helminth infections in both, humans and animals [7].

However, according to the Biopharmaceutics Classification System (BCS), PZQ belongs to Class II for its high permeability and low water solubility [8], thus being drug solubility the major barrier for the bioavailability of PZQ after its oral administration.

Several solid forms of PZQ have been reported, including polymorphs A [9], B [10], and C [11], as well as an amorphous (AM) [12]. More recently, additional new solid phases of the PZQ racemate have been reported, including Forms D, E and F, where the first two are crystalline and the last one is amorphous [13]. Additionally, the discovery of a novel crystalline form of PZQ was recently informed using high-pressure supercritical carbon dioxide [14]. PZQ has two known hydrates, a monohydrate (MH) [15] and a hemihydrate (HH) [16], and a hemihydrate has been reported for every drug enantiomer [17, 18]. Other solid forms of PZQ, obtained as solvates [19], cocrystals [20], a cyclodextrin complex [21], and solid-solid dispersions [22, 23] widen the landscape of the PZQ solid forms.

Hydrates may become suitable alternatives for drug formulation, especially if they display better pharmaceutical features than their

* Corresponding author.
** Corresponding author.
E-mail addresses: kaufman@iquir-conicet.gov.ar (T.S. Kaufman), maggio@iquir-conicet.gov.ar (R.M. Maggio).

https://doi.org/10.1016/j.heliyon.2022.e11317
Received 3 May 2022; Received in revised form 7 July 2022; Accepted 25 October 2022

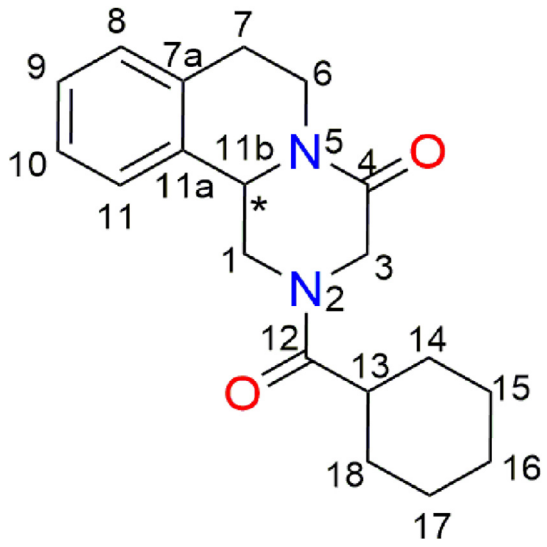

Figure 1. Chemical structure of PZQ, where the asterisk marks its stereogenic center.

corresponding anhydrates, such as processability and stability [24]. Molar mass stability is especially important when dealing with hygroscopic drugs [25]. The potential pharmaceutical applications of HH and MH could be justified in their better dissolution properties and their lower hygroscopicity with regards to the commercial Form A of PZQ.

Information about the stability of MH is limited and relates to the time the hydrate remained unaltered under given conditions [15]. On the other hand, stability studies have been previously conducted on HH at room temperature, at 50 °C under vacuum overnight, and up to 80 °C in a variable-temperature powder X-ray diffraction (PXRD) experiment, where Form B was observed. The latter polymorph was also detected when HH was submitted to mechanical stress (milling) [16]. Interestingly, however, these observations where not fully confirmed by concomitant DSC studies, where an additional polymorph was observed after the melting event of Form B. The intimate details about the mechanism behind such transition remain unknown.

Therefore, in order to add details to this fragmentary information and remove conflicting evidences, it is critical to revise the dehydration process of PZQ hydrates and acquire proper knowledge on the identity of all the species involved in the solid form changes and their impact on the dissolution performance of the solids.

Hot-stage (HS) attenuated total reflectance (ATR) coupled to mid infrared spectroscopy (MIR) spectroscopy can provide real-time information from thermally controlled processes or evolving thermally driven events. However, MIR spectra are complex and rich in information; therefore, their processing turns necessary the application of computational methods to extract the information from the data.

Multivariate curve resolution coupled to alternating least squares (MCR-ALS) is a chemometric tool especially suited to extract information from variable time-, temperature-, or pH-dependent evolving systems [26]. In this way, relevant features such as the abundance profiles of the different species involved throughout the process, along with spectral information of the corresponding pure species can be accessed.

Therefore, in order to gain a more detailed knowledge on the stability of praziquantel hydrates under thermal stress conditions, herein we report our results about the transformations of HH and MH when monitored using HS-ATR-MIR empowered by MCR-ALS, including the identity of the solid phases involved in the different transitions. Confirmation of these findings through PXRD and thermal methods, and the impact of thermal stress on the dissolution rates of the solids are also discussed.

2. Materials and methods

2.1. Chemicals

Racemic PZQ (USP grade) bulk drug was acquired from Unifarma S.A. (Buenos Aires, Argentina) and kept in a desiccator protected from the light. All chemicals used were of analytical grade and were used as received.

2.2. Preparation of the solid forms of PZQ

Forms A and MH were obtained from racemic commercial PZQ, following the procedure described in the literature [15].

Form B was obtained from racemic commercial PZQ following both, literature [10] and employing this ad-hoc procedure: A stainless-steel container with commercial PZQ (300 mg) was heated in a vacuum oven at 150 °C and 60 mm Hg for 30 min. The sample was placed in a desiccator and left to attain room temperature, obtaining a vitreous solid. No mass changes were observed during the whole treatment. Then, the total amount of the solid (≈300 mg) was transferred to a stainless-steel milling jar (2.0 × 2.2 cm, I.D. × H) equipped with stainless steel spheres (D = 3–6 mm) submitted to 25 Hz for 150 min in a Zonytest EJR 2000 vibratory tower (Rey & Ronzoni, Buenos Aires, Argentina) maintained at 20 °C and 40% RH. Both procedures yielded the same PXRD pattern, thus the second one was used as the default method (Figure S1).

The Form HH was obtained according to the literature [16] and using the following procedure: Distilled water (1 ml) was added to Form B (200 mg) and the mixture was left under stirring (35 rpm) at room temperature for 72 h. Both procedures yielded the same PXRD pattern and water content; thus, the second one was used as the default method (Figure S2).

The particle size of the solid samples was standardized by sieving before their further analysis; in all cases, the 100–140 mesh fractions were collected for use.

2.3. Instrumentation

The MIR spectra were acquired in a Shimadzu Prestige 21 FTIR spectrometer (Shimadzu Corp., Kyoto, Japan), in the absorbance mode (20 scans each), over a wavenumber range of 4000–600 cm^{-1} and at a resolution of 4 cm^{-1}. The ATR experiments were carried out with a diamond-based ATR accessory (GladiATR, Pike Technologies, Madison, USA), fitted with a Pike temperature control unit. Samples were measured in triplicate.

The NIR spectra were obtained with a NIRS DS2500 spectrometer (FOSS, Hillerod, Denmark). Every sample (300 mg) was placed in a quartz cup for solids and triplicate determinations were acquired in the 500–2500 nm range, in reflectance mode.

The DSC determinations were executed with a Linseis model PT1000 instrument (Linseis, Selb, Germany). The samples (3–5 mg) were placed in sealed aluminium pans perforated with a pin-hole to equilibrate pressure from the potential expansion of evolved gases or residual solvents. The pans were heated at 10 °C min^{-1} from 30 °C to 170 °C under a constant nitrogen flow (50 ml min^{-1}), employing an empty aluminium pan as a reference. The thermogravimetric analyses (TG) were carried out on a Shimadzu DTG-60H (Shimadzu, Kyoto, Japan) instrument. The samples (10 mg) were heated between 30 °C and 170 °C at a constant rate (10 °C min^{-1}), under a nitrogen purge (30 ml min^{-1}).

The PXRD patterns were obtained using a Panalytical MPD unit (Malvern Panalytical, Malvern, United Kingdom) equipped with a Cu anode, X-ray lenses, a Xe gas detector, a graphite monochromator and Soller parallel plates on the secondary beam. Measurements were made by adding the Kα1,2 signals, with vertical and horizontal slits (3 × 3 mm^2 beam area), in continuous scans (5 s per 0.02° 2θ increment) in the $10° < 2\theta < 105°$ range.

The cross-polarization/magic angle spinning (CP/MAS) ^{13}C ssNMR spectra were obtained at room temperature in a Bruker Ascend 400 MHz

spectrometer (Bruker BioSpin GmbH, Rheinstetten, Germany). The samples (200 mg) were packed into a standard zirconium (ZiO_2) rotor, equipped with Kel-F caps and the spectra were acquired at a rotation rate of 7 kHz; the contact time during the cross-polarization was 2 ms with a relaxation delay of 5 s. The chemical shifts are informed in parts per million (ppm), in the δ scale.

The intrinsic dissolution rate (IDR) studies were performed in previously degassed double distilled water (1000 ml), at 37 °C and a paddle rotation rate of 100 rpm. Aliquots of 3 ml were manually withdrawn with replacement, at 5, 10, 20, 30, 40, 50, and 60 min, using 10 μm filter tips for the sampling probe. The amount of dissolved PZQ was spectrophotometrically determined at 220 nm. The samples (150 mg) were prepared in a sample holder (I.D. = 13 mm), and subjected to pressure (2 T cm^{-2}) for 2 min in a hydraulic press (PerkinElmer, Norwalk, USA); the samples were analyzed in triplicate.

2.4. Chemometrics and graphics software

Chemometric analysis was carried out with the aid of MCR-ALS GUI 2.0 (available at https://mcrals.wordpress.com/download/), executed in Matlab R2015a (Mathworks, Natick, USA).

Data analysis and graphics were executed in OriginPRO v.8 (OriginLab, Northampton, USA), using original data of the instrumental signals in ASCII format. The chemical structure was drawn using the ChemOffice Pro v.16 software (Perking Elmer Informatics, Cambridge, USA).

3. Results and discussion

3.1. Characterization of the solids

The characterization of the PZQ solid forms was carried out using spectroscopic and diffractometric methodologies, including MIR, NIR, ssNMR (Figure S3) and PXRD (Figure S4). The spectra and diffractograms were in agreement with the literature (Supplementary material) [10, 15, 16]. The assignment of MIR and NIR spectra is presented herein, in order to allow further discussions.

The MIR spectrum of MH showed a wide band peaking at 3417 cm^{-1}, whereas HH displayed a sharp band at 3535 cm^{-1}; both signals were attributed to the OH group, indicating the presence of water in the corresponding structures. On the contrary, forms A and B lacked this signal, confirming their anhydrous nature (Table 1 and Figure 2).

Form A exhibited a well-defined double peak at 1620 and 1647 cm^{-1}, while B form showed two overlapped peaks at 1643 and 1631 cm^{-1}, attributable to the symmetric stretching mode of the heterocyclic carbonyl and to that of the carbonyl group joined to the cyclohexyl moiety. In comparison, HH exhibited a single sharp signal at 1620 cm^{-1}, while MH showed a broad band in the 1626 cm^{-1} region.

Finally, form A presented a broad peak with a shoulder at 762 cm^{-1}, in contrast to form B, MH and HH, which exhibited a signal at 758 cm^{-1} with lower intensity. Both signals are related to the *ortho*-substituted nature of the aromatic ring moiety of the drug.

Table 1. Assignment of the main MIR absorptions of forms A, B, HH and MH of PZQ.

Form A	Form B	HH	MH	Assignment
-	-	3483	3481	υ(OH
2926, 2848	2926–2956	2924, 2850	2926, 2850	υ_s(CH) and υ_{as}(CH)
1645, 1620	1643 1631	1634	1624	υ(C=O); amide
1445	1441	1433	1433	δ(C=C)
1418	1420	1416	1417	δ_s(CH); cyclic structure
1300	1298	1299	1296	υ(C–N)
1325, 1286, 1259, 1244 1209	1336, 1284, 1261, 1244 1217	1325, 1282, 1257, 1242 1209	1325, 1284, 1257, 1244 1209	δ(C–N); axial deformation; γ(CH)$COCH_2$N
762	758	758	760	γ(CH); aromatic –CH wagging of *ortho*-disubstituted aryl

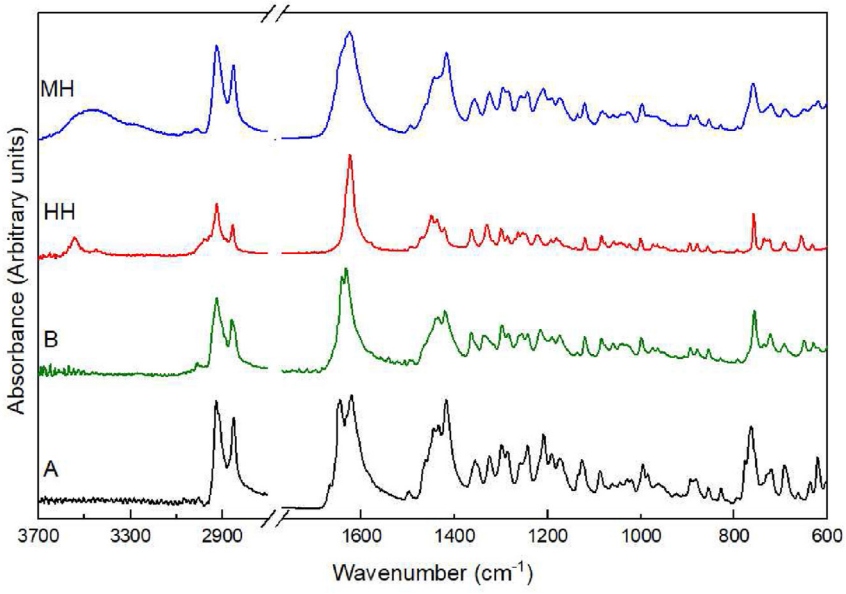

Figure 2. MIR spectra of the pure solid forms A (-), B (-), HH and MH (-) of PZQ (-).

Taking into account that water absorbs in the NIR region, this spectroscopy resulted relevant for the characterization of the hydrates and their differentiation from the corresponding anhydrous forms.

NIR spectroscopic analysis revealed some differential features among the solid forms of PZQ (Table 2 and Figure 3). Significant changes were observed in the zones 1390–1480 nm and 2290–2450 nm, that could be assigned to changes in the combinations of ArC-H, CH and CH_2 as the result of different packing of the solid forms of PZQ.

The region 2140–2170 nm, corresponding to the combination bands of the amide, also showed differential absorptions. Finally, MH and HH presented an elastic band of OH in the region 1870–1920 nm, attributable to the water of hydration; on the contrary, forms A and B lacked this band, due to their anhydrous nature, confirming the observations of the MIR spectra.

Additionally, the IDR values (Figure 4) for Forms HH and MH (0.0290 ± 0.0010 and 0.0250 ± 0.0008 mg cm^{-2} min^{-1}, respectively) proved to be statistically different among them ($t_{obs} = 23.09$; $t_{crit\ (10,\ 0.05)} = 1.79$), and substantially higher than Form A (0.0172 ± 0.0003 mg cm^{-2} min^{-1}). Considering that HH and MH exhibit promissory dissolution properties, these novel phases were assessed, looking for amorphization or changes to less soluble forms.

3.2. Thermal analysis of HH and MH

The first step of any stability study requires unveiling the nature of the transformations suffered by each of the phases. Thus, a thermal analysis based on DSC and TG was carried out on HH and MH. The DSC thermogram of MH (Figure 5A) showed two endothermic transitions; the first one had an onset at 78 °C, peaked at 90 °C and continued with a shoulder that ended after 125 °C, being related to water loss.

This was confirmed by TG analysis (Figure 5B), where MH displayed a well-defined mass loss of about 5.4%, which began around 78 °C and ended after 125 °C. This is consistent with the theoretical mass loss of a monohydrate (5.45%). The second transition, with $T_{onset} = 130$ °C ($\Delta H = 104.13$ J g^{-1}), resembles the behavior of Form A ($T_{onset} = 135$ °C) and takes place with a similar heat of fusion ($\Delta H = 91.2$ J g^{-1}).

Previous DSC studies revealed that HH undergoes a slow change to Form B, which melts and suffers transformation into an additional Form [16]. Thus, confirmatory DSC studies were run, observing that the HH scan presented three endothermic transitions, where the first one ($T_{onset} = 60$ °C; $\Delta H = 77.3$ J g^{-1}) was related to a dehydration event, as confirmed by TG (gradual 2.5% mass loss between ~60 and 90 °C). The second endothermic event, observed at $T_{onset} = 104$ °C ($\Delta H = 27.43$ J g^{-1}), can be associated with the melting of Form B ($T_{onset} = 105$ °C; $\Delta H = 59.0$ J g^{-1}), thus suggesting a partial conversion of HH to Form B. Finally, the last peak (T_{onset} 128 °C; $\Delta H = 33.99$ J g^{-1}) could be related to the melting event of Form A, according to its temperature and enthalpy values. These observations were in full agreement with the literature [16].

3.3. Monitoring HH and MH phase transformations by HS-ATR-MIR

The observed transitions during the DSC and TG analyses suggested that MH undergoes a single-step transformation, whereas HH suffers a sequential two-stage conversion. However, despite that the nature of the events and the species involved could be interpreted from their melting points, the observed differences in temperature and enthalpy values, although minor, turned necessary further analysis to ascertain the identity of the involved species and their corresponding transition temperatures. Therefore, HH and MH were submitted to HS-ATR-MIR analysis.

The monitoring setup enabled heating the samples on the ATR stage at a rate of 5 °C min^{-1} (30–145 °C), while acquiring MIR spectra (3500-600 cm^{-1}) every minute. MCR-ALS was then applied to the so obtained spectra in order to resolve the high spectral overlapping evidenced among the species, which impeded knowing their actual number, along with their nature and the corresponding temperature transitions.

Table 2. Assignment of main NIR absorptions of forms A, B, HH and MH of PZQ.

Form A	Form B	HH	MH	Assignment
1150, 1205	1440	1137, 1197	1149, 1204	2nd CH overtone
1387	1384	1381	1393	CH; combination
-	-	1401	1407	1st OH overtone
1678	1681	1682	1682	ArC-H; CH_2CO
1702	1712	1706	1708	1st CH overtone
1756	1755	1750	1755	CH_2; combination
-	-	1924	1926	OH stretch; combination
2142	2143	2145	2140	Amide combination

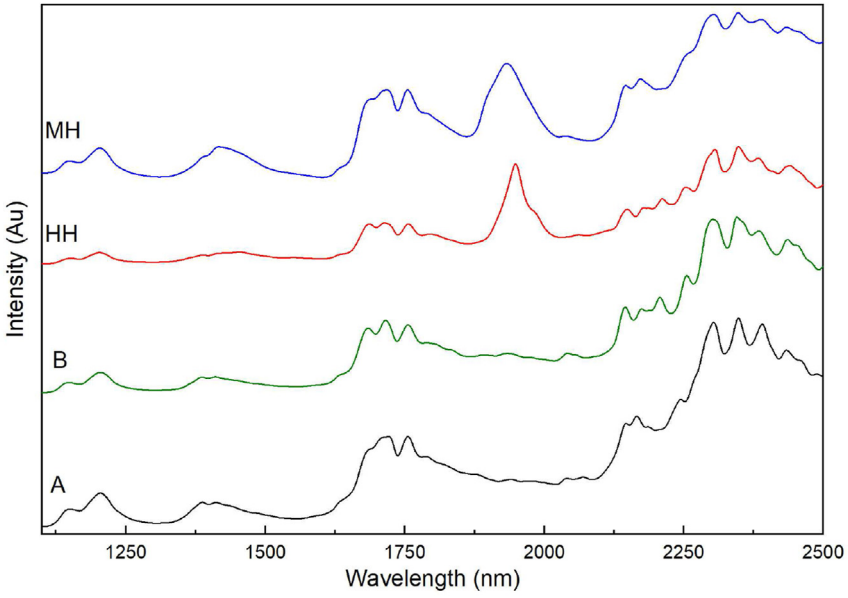

Figure 3. NIR spectra of the solid forms A (-), B (-), HH (-) and MH (-) of PZQ.

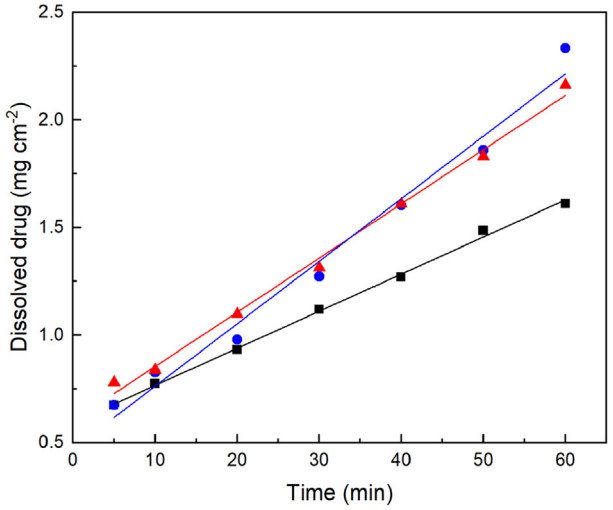

Figure 4. IDR data for HH (-●-), MH (-▲-) and Form A (-■-), along with their corresponding fitted lines.

To properly run the MCR-ALS algorithm, the data were pre-treated, applying a baseline correction, a maximum absorption normalization and the Savitzky-Golay filter. In addition, the spectra were edited, removing the poorly informative 2700-1700 cm^{-1} region. In order to confer physicochemical sense to the results, some restrictions were applied to the MCR-ALS algorithm; these included non-negativity in the spectral and concentration profiles, as well as unimodality in the concentration mode and the system closure.

The number of components was established as four by the use of the method of the explained variance after the single value decomposition (SVD); this was in complete agreement with the number of observed transitions (three) in the thermal analysis experiment. Therefore, the MCR algorithm was initialized with four spectra, including those of the initial (HH) and final fused form (FUS), as well as two random vectors, which were used in place of the unknown spectra of the second and third components.

MCR-ALS solved the matrix of experimental data and provided estimated spectral (S1, S2, S3, and S4) and concentration profiles of four species (SD = 0.14; total R^2 = 99.5%). The "pure spectra" provided by MCR-ALS were visually and statistically compared by correlation analysis to the spectra of the pure forms A, B, MH, HH and FUS.

This procedure enabled the identification of such species as HH, Form B, Form A and FUS for S1, S2, S3 and S4, respectively (Figure 6). These results revealed that dehydration of HH initially generates polymorph B; in turn, the latter is transformed into Form A, which finally melts to deliver FUS.

The determination of the characteristics and nature of the transitions among the different forms was carried out by examination of the corresponding abundance profiles, which gave information about the transition temperatures and conversion ratios (Figure 7). Thus, it was detected that under this thermal treatment form HH is totally converted into form B at 90 °C; this event is followed by a second transformation at 107 °C, which quantitatively yields form A at about 115 °C. Further heating triggers the last transition, observed at 136 °C, which corresponds to the complete fusion of the solid; the complete series of events is in full concordance with the DSC experiment.

It was established that the transformation of Form HH occurs according to a two-step mechanism, where the consecutive formation of polymorph B and Form A takes place. This is followed by the melting of Form A to give a stable fused product. An analysis of the MIR spectra obtained from MCR-ALS during thermal treatment was carried out in order to obtain a rational explanation of the reaction scheme. The first observed change was the disappearance of the signal assigned to υ(OH) at 3485 cm^{-1} due to the loss of water during the transformation of HH to Form B. Simultaneously, it was observed the splitting of υ(C–O) of the amide group (1634 cm^{-1}) in two different vibrations (1643 and 1631 cm^{-1}) and the displacement of one of them to a higher wavenumber, showing the gain of rigidity in the covalent bonds. The aromatic ring also evidenced changes, where C=C showed an increment in the bond energy (1433–1441cm^{-1}), implying that it is involved in the change of the crystalline structure.

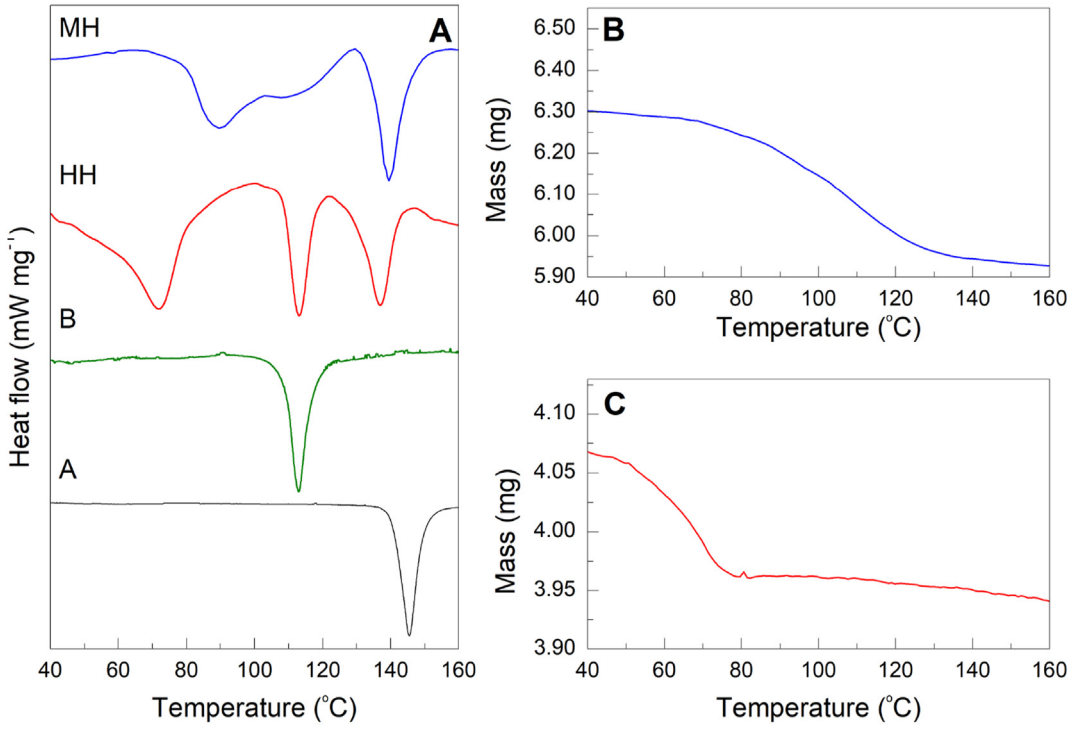

Figure 5. DSC thermograms of Forms A (-), B (-), HH (-) and MH (-) of PZQ (A). TG analysis of MH (-, B) and HH (-, C).

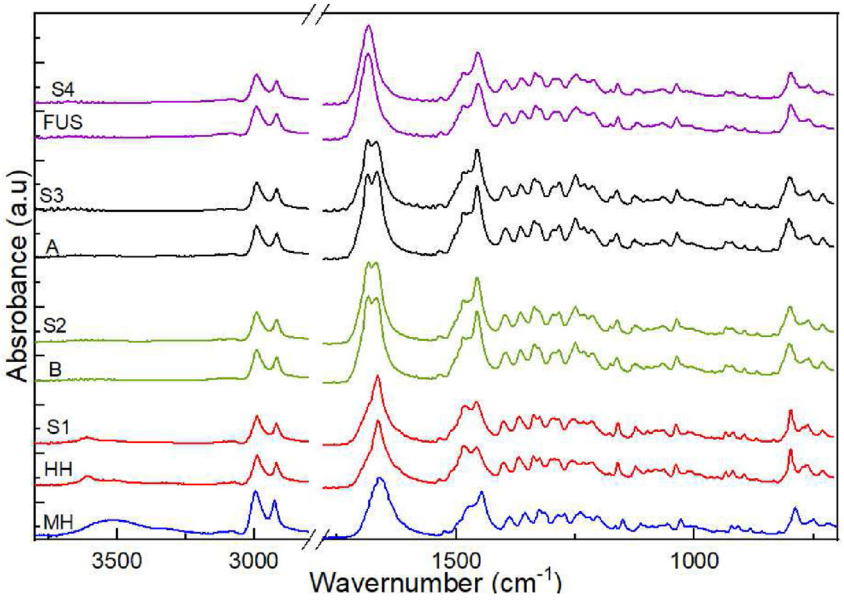

Figure 6. Pairwise comparison between the reference spectra and those provided by the MCR-ALS deconvolution; S1 (-) versus HH (-); S2 (-) vs B (-); S3 (-) vs A (-) and S4 (-) vs FUS (-). The reference spectrum MH (-) stand-alone.

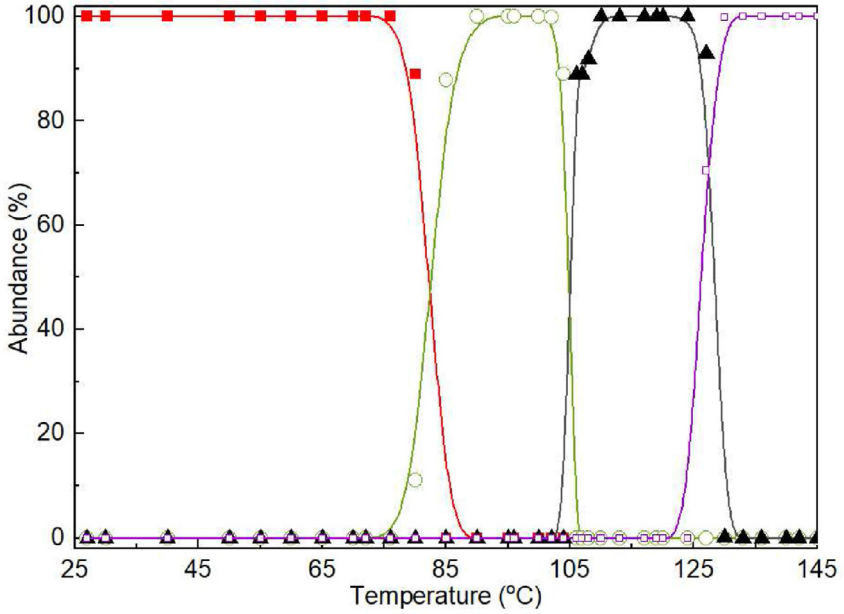

Figure 7. Concentration profiles of the different pure ALS species for HH (-■-), B (-○-), A (-▲-) and FUS (-□-) obtained by MCR-ALS during the heating process.

Subsequently, the transformation of Form B into Form A took place; as a result, the υ(C–O) of the amide group conserved both signals but it augmented the difference of their energy, shifting from 1643 and 1631 cm^{-1} to 1645 and 1620 cm^{-1}, respectively. The aromatic ring evidenced a change that continued the tendency found from HH to B, where the C=C bond evidenced an increment in energy (1441–1445 cm^{-1}), showing a progressive change in the crystalline arrangement. A further analysis of the structural changes experimented during the transformation solid forms should be completed in future works with Density functional theory (DFT) calculations.

An analogous scheme was employed for the HS-ATR-MIR analysis of MH. The solid was heated at rate of 5 °C min^{-1} and monitored between 30-145 °C, and the so obtained spectra were also analyzed using the MCR-ALS tool. The data matrix contained 17 temperature sensors for spectra containing 1369 wavenumber sensors each, and the spectral pretreatment was the same applied above.

The number of expected components was established by examining the explained variance of the data matrix after SVD, which revealed that three components accounted for more than 97% of the total variance. The spectrum of MH was used as the initial estimation of the starting species (S1), while a random vector was employed for the intermediate species (S2) and a spectrum of FUS was included to account for the remaining species (S3).

To ensure an MCR-ALS resolution embedded with physicochemical sense, non-negativity restrictions were applied to spectral and concentration modes, while the unimodality restriction and the closure condition were applied only to the concentration profiles.

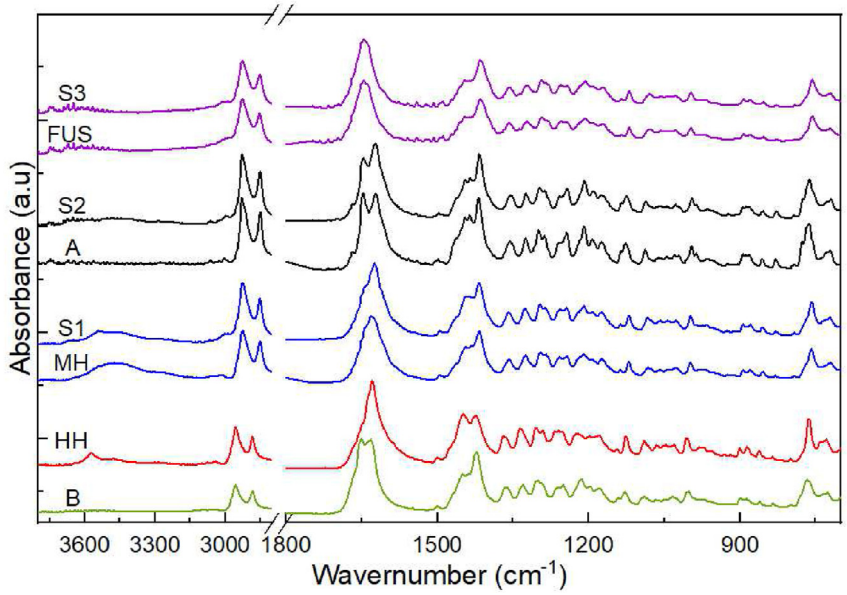

Figure 8. Pairwise comparison among the reference spectra and those provided by the MCR-ALS deconvolution; S1 (-) vs MH (-); S2 (-) vs A (-) and S3 (-) vs. FUS (-). Reference spectra of B (-) and HH (-) stand-alone.

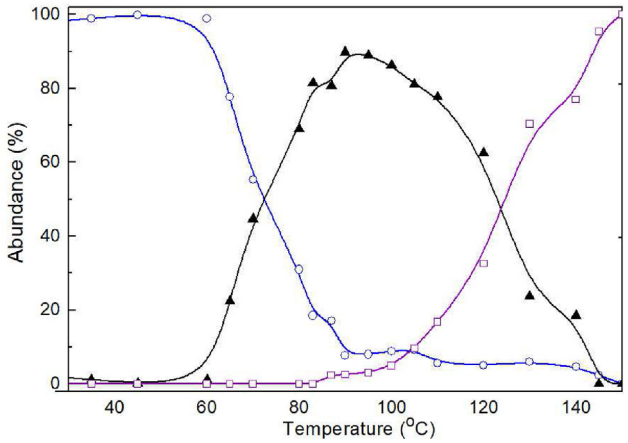

Figure 9. Heat-driven transformation of MH. Concentration profiles of the pure species obtained by MCR-ALS during the heating process. MH (-○-); Form A (-▲-) and FUS (-□-).

Data resolution was obtained after 20 iterations (SD = 0.01; total R^2 = 99.88%). The species were identified by pairwise statistical comparisons between the MIR spectra of the pure species and those obtained by MCR-ALS, through the corresponding correlation coefficients (R).

As expected, S1 and S3 were assimilated to MH and FUS, respectively, while the intermediate (S2) showed very high similarity with Form A. The comparisons between the MCR-ALS spectral profiles and the best-matched spectra of the corresponding pure forms are shown in Figure 8.

Once the species were identified, the thermal data were analyzed with regards to their concentration profiles. Accordingly, it was concluded that MH underwent a dehydration process starting approximately after 70 °C (Figure 9), which resulted in the concomitant formation of Form A, which reached a maximum around 90 °C (90%), in full agreement with DSC observations (Figure 5A). A melting event takes place as the temperature increases, concomitantly with the disappearance of Form A; this event becomes relevant after about 125 °C.

The results of the thermal behaviour of MH were in good agreement with those observed during the thermal analysis, where a low heat transfer event and mass loss were initially observed (70 °C) in DSC and TG respectively. This correlated with the transition of MH to Form A detected by MIR/MCR-ALS at the same temperature. As the temperature raised, an endothermic event of greater magnitude took place, compatible with the melting event observed by MIR/MCR-ALS.

Compared to DSC observations, the almost complete transitions detected in the HS-ATR-MIR analysis for HH and MH may result from different heating transference (rates and mass). When lower rates are applied, more time is given to allow form conversion, resulting in a higher degree of transformation between the solid phases.

MCR-ALS also suggested that, under analogous thermal conditions, MH undergoes a single-step dehydration event, to afford Form A gradually, the more stable polymorph of PZQ. As in the case of HH, the first change was the disappearance of the signal assigned to υ(OH) at 3481, due to water loss during the conversion of MH to Form A. Simultaneously, the υ(C=O) of the amide group (1624 cm^{-1}) split in two vibrations with displacements to higher (1645 cm^{-1}) and lower (1620 cm^{-1}) wavenumbers, observation that was on accord to the two different conformations in the unit cell. The signal of υ(C–N) moved from 1296 to 1300 cm^{-1}, revealing a higher restriction to the movements of the amide group. The aromatic ring also showed an increment in the C=C bond energy (1433–1445 cm^{-1}), implying that it is involved in the change of the crystalline structure.

In order to confirm the transformation of HH and MH to Form A under HS-ATR-MIR, the thermal treatment was repeated up to 124 °C and suddenly stopped. The so obtained samples were submitted to PXRD analysis confirming the obtained structure as Form A.

3.4. Evaluation of HH and MH phase transformations by in simulated bulk processing. Impact on dissolution rate

In order to evaluate the impact of the transformation of the hydrates under processing-like conditions, both forms (~1 g) were subjected to heating at a constant temperature, in the absence of oxygen (N_2 atmosphere) to prevent oxidation, using a vacuum oven. The hemihydrate was heated at 84 and 124 °C for a period of 20 min (HH84 and HH124, respectively), whereas MH was kept 124 °C for 20 min (MH124).

In agreement with the MCR-ALS prediction, that above 80 °C HH undergoes transformation into Form B, the thermogram HH84 revealed significant presence of Form B (~85%) and a small initial endotherm that could be compatible with the glass transition of an amorphous state. This

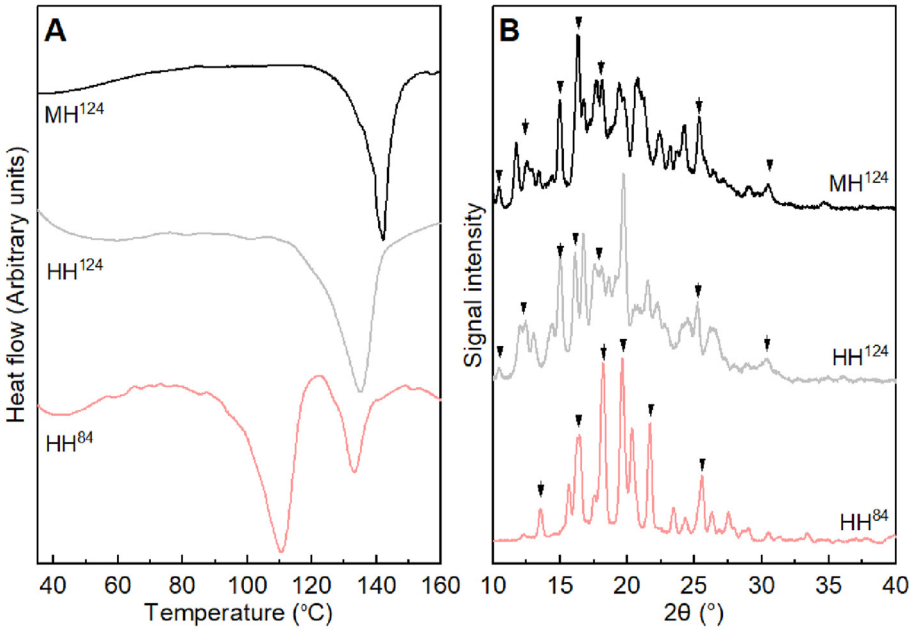

Figure 10. DSC thermograms (A) and PXRD diffractograms (B) of the solid samples MH84 (-), HH124 (-) and HH84 (-) of PZQ, major signals of pure forms A and B (▼).

was further confirmed by the diffractogram of HH84, which evidenced massive formation of Form B, along with a small baseline shift (Figure 10).

On the other hand, the DSC thermogram of HH124 evidenced a single well-defined peak, related to the fusion of Form A (~80%) along with a small event compatible with a glass transition as previously observed. Interestingly, no signals of Form B were detected. These results were confirmed by the PXRD study, which showed signals compatible with Form A, over a more intensely shifted baseline, correlated to the content of the amorphized drug.

Not unexpectedly, the DSC thermogram of MH124 was similar to that of HH124, and its diffractogram corroborated the predominant presence of Form A, along amorphized drug, as stemmed from the accompanying small halo.

The appearance of an amorphous state under these conditions can be explained by the sudden nature of the heat treatment, which forces a rapid water loss without giving time for the corresponding rearrangement of the crystal lattice, unlike the gradual temperature increase which takes place during the DSC and HS-ATR-MIR treatments. The influence of such heat treatment on the dissolution of the solids as a performance evaluation tool was assessed. When compared to the dissolution of HH, the sample HH84 showed both an increase in the amount of drug dissolved at early times (10 min) and an increase in the dissolution rate (Figure 11A). This is consistent with the heat-

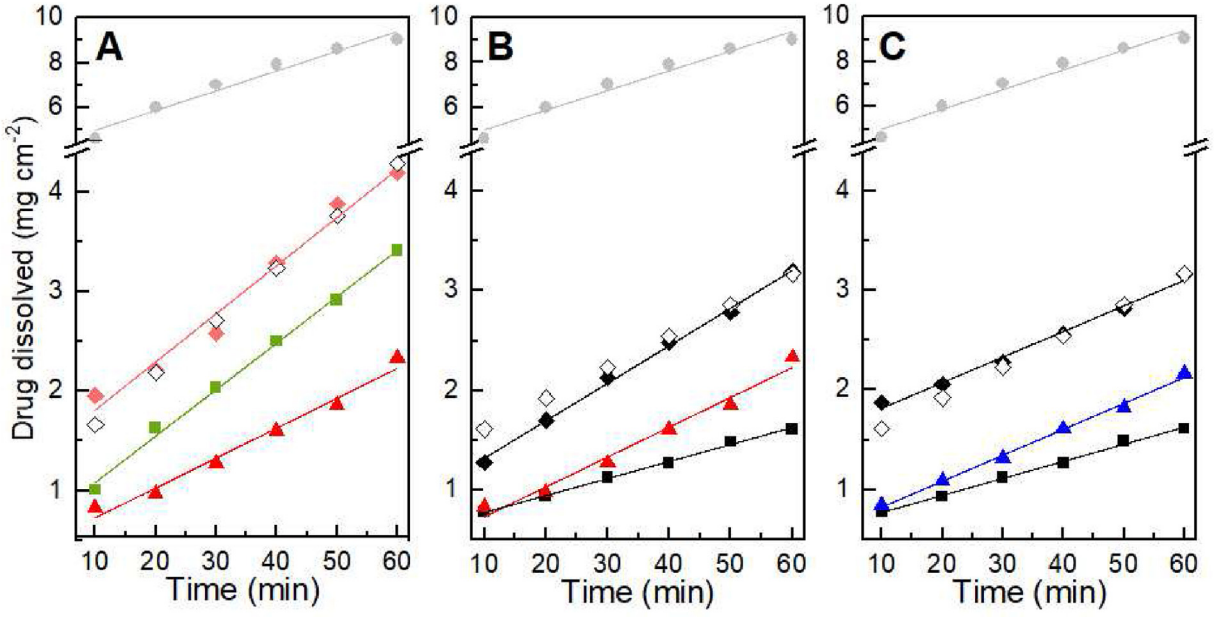

Figure 11. IDR of (A) HH84 (♦), simulated HH84 mixture (◊), AM (●), Form B (■) and HH (▲) (B) HH124 (♦), simulated HH124 mixture (◊), AM (●), Form A (■), HH (▲); and (C), MH124 (♦), simulated MH124 mixture (◊), AM (●), Form A (■) and MH (▲).

promoted formation of polymorph B and the presence of ~15% of an amorphous phase (AM), both with higher IDR (Figure 11A). The existence of such a transformation at temperatures around 80 °C was predicted by MCR-ALS and is supported by PXRD and DSC observations of this heat-stressed sample. Additionally, when the IDR profile of a mixture of Form B:AM (85:15) was reconstructed from the IDR curves of the pure forms, it showed no significant differences with that of HH84.

Analogously, previous PXRD and DSC results predicted a minor but significant content of AM in sample HH124. Therefore, it was not surprise that comparison between the IDR curves of HH124 and the IDR profile of a Form A:AM (80:20) simulated mixture showed no significant differences (Figure 11B). The lower overall dissolution of HH124 in comparison to HH84 could stem from the strong influence of Form A, which exhibits the lowest dissolution rate and whose abundance in the mixture is high (~80%).

In agreement with the DSC and PXRD studies, the intrinsic dissolution curve of MH124, the MH sample subjected to the 124 °C treatment (Figure 11C) was comparable to the results of HH124 (Figure 11B). The IDR curve of MH124 showed early dissolution times governed by the presence of AM and an overall dissolution behaviour (slope) driven by its content of Form A (about ~80%). Thus, the IDR curve of MH124 displayed no significant differences when compared with the profile of a Form A:AM (80:20) simulated mixture, validating these observations.

4. Conclusions

The solid-state transformations of HH and MH under heat stress were monitored by HS-ATR-MIR empowered by MCR-ALS and by DSC. This combination furnished the spectral and concentration profiles of the involved components along with qualitative and quantitative information, which gave access to a more detailed description of the thermal events and an unequivocal identification of the participating species. It was established that the transformation of Form HH occurs according to a two-step mechanism, where the consecutive formation of polymorph B and Form A takes place. This is followed by the melting of Form A to give a stable fused product. MCR-ALS also suggested that, under analogous thermal conditions, MH undergoes a single-step dehydration event, to gradually afford Form A, the more stable polymorph of PZQ.

When HH and MH were submitted to thermal stress displayed significant changes in their dissolution behaviour. Thermal analysis and PXRD afforded information regarding composition of stressed samples at 84 and 124 °C, confirming the hypotheses related to phase changes established by MCR-ALS.

Taken together, these results suggest that HS-ATR-MIR spectroscopy coupled to MCR-ALS is a suitable approach to monitor the stability of hydrates and their fate under thermal stress conditions; this tool was able to identify the species involved in multiple and complex solid-state transformations.

Declarations

Author contribution statement

Duvernis Salazar-Rojas, Teodoro S. Kaufman, Rubén M. Maggio: Conceived and designed the experiments; Performed the experiments; Analyzed and interpreted the data; Contributed reagents, materials, analysis tools or data; Wrote the paper.

Funding statement

This work was supported by Consejo Nacional de Investigaciones Científicas y Técnicas (PUE06-IQUIR), and by Universidad Nacional de Rosario (BIO572 and 80020190300200UR).

Data availability statement

Data included in article/supplementary material/referenced in article.

Declaration of interests statement

The authors declare no conflict of interest.

Additional information

Supplementary content related to this article has been published online at https://doi.org/10.1016/j.heliyon.2022.e11317.

References

[1] IUPAC, Polymorphic Transition, Blackwell, Oxford, 2008.
[2] J. Wardrop, D. Law, Y. Qiu, K. Engh, L. Faitsch, C. Ling, Influence of solid phase and formulation processing on stability of abbott-232 tablet formulations, J. Pharmacol. Sci. 95 (2006) 2380–2392.
[3] S. Piqueras, L. Duponchel, R. Tauler, A. De Juan, Monitoring polymorphic transformations by using in situ Raman hyperspectral imaging and image multiset analysis, Anal. Chim. Acta 819 (2014) 15–25.
[4] M. Hong, J. Chen, H. Zhou, H. Xu, G. Ren, Investigation of a solution-mediated phase transformation of pranlukast DMF solvate to hemihydrate, Cryst. Res. Technol. 52 (2017), 1700045.
[5] A.M. Healy, Z.A. Worku, D. Kumar, A.M. Madi, Pharmaceutical solvates, hydrates and amorphous forms: a special emphasis on cocrystals, Adv. Drug Deliv. Rev. 117 (2017) 25–46.
[6] D. Cioli, L. Pica-Mattoccia, A. Basso, A. Guidi, Schistosomiasis control: praziquantel forever? Mol. Biochem. Parasitol. 195 (2014) 23–29.
[7] J. Wei, F. Cheng, Q. Qun Nurbek, S.-D. Xu, L.-F. Sun, X.-K. Han, L.-L. Muhan, Han Irixiati, P. Jie, K.-J. Zhang, I.J. Chai, Epidemiological evaluations of the efficacy of slow-released praziquantel-medicated bars for dogs in the prevention and control of cystic echinococcosis in man and animals, Parasitol, Bar. Int. 54 (2005) 231–236.
[8] M. Lindenberg, S. Kopp, J.B. Dressman, Classification of orally administered drugs on the World Health Organization model list of essential medicines according to the biopharmaceutics classification system, Eur. J. Pharm. Biopharm. 58 (2004) 265–278.
[9] J.C. Espinosa-Lara, D. Guzman-Villanueva, I. Arenas-Garc, D. Herrera-Ruiz, P. Roma, H. Morales-Rojas, H. Ho, Cocrystals of active pharmaceutical ingredients-praziquantel in combination with oxalic, malonic, succinic, maleic, fumaric, glutaric, adipic, and pimelic acids, Cryst. Growth Des. 13 (2013) 169–185.
[10] D. Zanolla, B. Perissutti, N. Passerini, M.R. Chierotti, D. Hasa, D. Voinovich, L. Gigli, N. Demitri, S. Geremia, J. Keiser, P. Cerreia Vioglio, B. Albertini, A new soluble and bioactive polymorph of praziquantel, Eur. J. Pharm. Biopharm. 127 (2018) 19–28.
[11] D. Zanolla, B. Perissutti, P.C. Vioglio, M.R. Chierotti, L. Gigli, N. Demitri, N. Passerini, B. Albertini, E. Franceschinis, J. Keiser, D. Voinovich, Exploring mechanochemical parameters using a DoE approach: crystal structure solution from synchrotron XRPD and characterization of a new praziquantel polymorph, Eur. J. Pharmaceut. Sci. 140 (2019), 105084.
[12] E.D. Costa, J. Priotti, S. Orlandi, D. Leonardi, M.C. Lamas, T.G. Nunes, H.P. Diogo, C.J. Salomon, M.J. Ferreira, Unexpected solvent impact in the crystallinity of praziquantel/poly(vinylpyrrolidone) formulations. A solubility, DSC and solid-state NMR study, Int. J. Pharm. 511 (2016) 983–993.
[13] B. Saikia, A. Seidel-Morgenstern, H. Lorenz, Role of Mechanochemistry in Solid form selection and identification of the drug praziquantel, Cryst, Growth Des 10 (2021) 5854–5861.
[14] L. MacEachern, A. Kermanshahi-pour, M. Mirmehrabi, Transformation under pressure: discovery of a novel crystalline form of anthelmintic drug praziquantel using high-pressure supercritical carbon dioxide, Int. J. Pharm. 619 (2022), 121723.
[15] D. Salazar-Rojas, R.M. Maggio, T.S. Kaufman, Preparation and characterization of a new solid form of praziquantel, an essential anthelmintic drug. Praziquantel racemic monohydrate, Eur. J. Pharmaceut. Sci. 146 (2020), 105267.
[16] D. Zanolla, D. Hasa, M. Arhangelskis, G. Schneider-Rauber, M.R. Chierotti, J. Keiser, D. Voinovich, W. Jones, B. Perissutti, Mechanochemical formation of racemic praziquantel hemihydrate with improved biopharmaceutical properties, Pharmaceutics 12 (2020) 289.
[17] T. Meyer, H. Sekljic, S. Fuchs, H. Bothe, D. Schollmeyer, C. Miculka, Taste , A new incentive to switch to (R)-praziquantel in schistosomiasis treatment, PLoS Neglected Trop. Dis. 3 (2009) 3–7.
[18] Y. Liu, X. Wang, J.-K. Wang, C.B. Ching, Investigation of the phase diagrams of chiral praziquantel, Chirality 18 (2006) 259–264.
[19] D. Zanolla, L. Gigli, D. Hasa, M.R. Chierotti, M. Arhangelskis, N. Demitri, W. Jones, D. Voinovich, B. Perissutti, Article mechanochemical synthesis and physicochemical characterization of previously unreported praziquantel solvates with 2-pyrrolidone and acetic acid, Pharmaceutics 13 (2021) 1606.

[20] O. Sanchez-Guadarrama, F. Mendoza-navarro, A. Cedillo-cruz, H. Jung-cook, I. Arenas-garc, A. Delgado-d, D. Herrera-ruiz, H. Morales-rojas, H. Ho, Chiral resolution of RS-praziquantel via diastereomeric co-crystal pair formation with L-malic acid, Cryst. Growth Des. 16 (2015) 307–314.
[21] M. Cugovčan, J. Jablan, J. Lovrić, D. Cinčić, N. Galić, M. Jug, Biopharmaceutical characterization of praziquantel cocrystals and cyclodextrin complexes prepared by grinding, J. Pharm. Biomed. Anal. 137 (2017) 42–53.
[22] D. Zanolla, B. Perissutti, N. Passerini, S. Invernizzi, D. Voinovich, S. Bertoni, C. Melegari, G. Millotti, B. Albertini, Milling and comilling praziquantel at cryogenic and room temperatures: assessment of the process-induced effects on drug properties, J. Pharm. Biomed. Anal. 153 (2018) 82–89.
[23] L. Di Marzio, A. Borrego-Sánchez, M. Felaco, M.E. Pacinelli, J. Gómez-Morales, N. d'Avanzo, C.I. Sainz-Díaz, C. Celia, C. Viseras, Praziquantel-loaded calcite crystals: synthesis, physicochemical characterization, and biopharmaceutical properties of inorganic biomaterials for drug delivery, J. Drug Deliv. Sci. Technol. 68 (2022).
[24] U.J. Griesser, The Importance of Solvates, Polymorphism, 2006, pp. 211–233.
[25] R.K. Khankari, D.J.W. Grant, Pharmaceutical hydrates, Thermochim. Acta 248 (1995) 61–79.
[26] M. Garrido, M. Larrechi, Multivariate curve resolution-alternating least squares (MCR-ALS) applied to spectroscopic data from monitoring chemical reactions processes, Anal. Bioanal. Chem. 390 (2008) 2059–2066.